Carbohydrate Polymers 118 (2015) 199–208

Contents lists available at ScienceDirect

Carbohydrate Polymers

journal homepage: www.elsevier.com/locate/carbpol

In situ mapping of the effect of additional mutations on starch granule structure in amylose-extender (*ae*) maize kernels

Dongli Liu[a,1], Nikolaus Wellner[b], Mary L. Parker[b], Victor J. Morris[b], Fang Cheng[a,*]

[a] College of Biosystems Engineering and Food Science, Zhejiang University, Hangzhou 310058, PR China
[b] Institute of Food Research, Norwich NR4 7UA, UK

ARTICLE INFO

Article history:
Received 3 July 2014
Received in revised form 6 November 2014
Accepted 9 November 2014
Available online 18 November 2014

Keywords:
In situ starch granule structure
Optical microscopy
FTIR imaging
GEMS-0067
wx-ae maize mutants

ABSTRACT

Optical (KI/I_2-staining, polarised) and FTIR microscopy has been used to monitor starch granule structure within wild-type (*wt*), *GEMS-0067* and waxy-amylose-extender (*wx-ae*) maize mutant kernels. In the *GEMS-0067* mutant containing the high amylose modifier (HAM) gene(s) plus the recessive *ae* gene, structural heterogeneity characteristic of the *ae* mutation was reduced markedly. However, enhanced variation in granule shape and size was observed distributed spatially within the kernel, which appears to be related to new heterogeneity in internal starch granule structure. In *wx-ae* starch mutants the *ae* gene led to heterogeneity of starch granule structure equivalent to that in single *ae* mutants, plus new structural heterogeneity coincident with novel induced variation in granule size and shape.

1. Introduction

Considerable progress has been made into determining the internal structure of starch granules. Native starches generally contain two polysaccharides called amylose and amylopectin. Amylose is an essentially linear molecule, considered to arise principally from the amorphous regions within the starch granule. Amylopectin is a highly-branched molecule that is considered to arise from the crystalline regions within the granule. The native starch granules exhibit a Maltese Cross pattern when observed under polarised light, which indicates that there is a radial orientation of the crystallites within the granule (Pérez & Bertoft, 2010). Wild-type (*wt*) maize starch yields around 30% amylose and 70% amylopectin. The ratio of amylose to amylopectin varies over a very wide range in different mutant maize starches.

Mutations in biosynthetic enzymes yield 'low-' and 'high-amylose' starches. There is increased interest in defining the changes in granule structure that result from selected mutations in starch biosynthesis. However, it cannot be assumed, even for individual mutations, that the mutations result in a homogeneous population of starch granules. Even isogenic mutants (*e.g.* amylose-extender (*ae*) maize) show heterogeneity in structure within populations of isolated starch granules (Cai, Zhao, Huang, Chen, & Wei, 2014; Chen, Yu, Chen, & Li, 2006; Evans, McNish, & Thompson, 2003; Katz, Furcsik, Tenbarge, Hauber, & Friedman, 1993).

The *ae* mutation involves the branching enzyme SBE IIb, and the resultant starch yields higher levels of amylose (Wu, Campbell, Yen, Wicks, & Ibrahim, 2009), together with amylopectin and some intermediate material (Pérez & Bertoft, 2010). To understand the structural variability of isolated *ae* granules, it is useful to map the structure of starch granules *in situ* within individual endosperm cells of the kernel. Such mapping documents spatial changes in starch structure arising from growth and development of the kernel. Starch granules present in cells progressively adjacent to the aleurone of the kernel are deposited later during the growth and development of the kernel (Watson, 1987). As such they will illustrate the effects of local changes in biochemistry within the cells during growth. Comparison of starch structures within the kernel with isolated starch structures gives insight into changes or losses that could occur on starch isolation.

Studies on the effect of the *ae* mutation on the distribution of granule structures within kernels build on previous *in situ* imaging of starch in dry seeds (Matsushima, Maekawa, Fujita, & Sakamoto, 2010; Parker, Kirby, & Morris, 2008; Wellner, Georget, Parker, & Morris, 2011; Zhu et al., 2012). Higher-resolution studies of *ae* maize kernels demonstrated and characterised granule heterogeneity within the kernel (Wellner et al., 2011) mirroring that

* Corresponding author. Tel.: +86 571 88982713; fax: +86 571 88982713.
E-mail address: fcheng@zju.edu.cn (F. Cheng).
[1] Current address: College of Food Science and Technology, Hainan University, Haikou 570228, PR China.

http://dx.doi.org/10.1016/j.carbpol.2014.11.006
0144-8617/

observed for isolated starches (Chen et al., 2006; Evans et al., 2003; Katz et al., 1993). Recent investigations (Gérard, Colonna, Bouchet, Gallant, & Planchot, 2001; Liu et al., 2013) have revealed the ultrastructural origins of this structural heterogeneity. These studies suggested that optical staining could be used to screen and map changes in granule structure within kernels.

The present study uses KI/I_2 staining to explore effects of double mutations on granule structure for *GEMS-0067* and *wx-ae* mutants. *GEMS-0067* contains the *ae* gene together with high-amylose modifier (HAM) gene(s), which might be expected to reduce structural heterogeneity induced by the *ae* mutation. Within *wx-ae* mutants, the *ae* gene will alter assembly of the ordered structure within the granule, whereas the *wx* gene is not involved in the biosynthesis of branched amylopectin-based structures. It is therefore interesting to establish whether the combined effects of these mutations are additive, synergistic or antagonistic. Fourier transform infrared (FTIR) microscopy has been used for additional characterisation of these double mutants.

2. Materials and methods

Kernels of *wt* maize (cultivar Oh 43) and the high-amylose *ae* mutant in an Oh 43 background were provided by Dr. K. Denyer (John Innes Centre, Norwich, UK) and Professor C. Weil (Department of Agronomy, Purdue University, West Lafayette, USA). Kernels of high-amylose *GEMS-0067* maize mutants (Reg. no. GP-550, Accession PI 643420) were generously supplied by the North Central Regional Plant Introduction Station (NCRPIS), part of the United States Germplasm System (NPGS). Kernels of *wx-ae* (14-7-19 7520) maize mutants were kindly provided by Dr. Véronique Planchot (INRA Angers – Nantes, France). All seeds used in this study were mature and the data presented is characteristic of studies made on 5–6 seeds.

2.1. Maize kernel sections

To investigate the spatial distribution of starch structures within kernels, sections were cut from three different locations within the kernel (Fig. 1a) using methods described elsewhere (Liu et al., 2013). Kernels were cut in half along the axis (L), and positioned to cut blocks and sections just below the crown (T1), mid-kernel (T2), and the lower part of the kernel (T3) (Fig. 1a). Rough surfaces were planed with a glass knife to generate a polished mirror-like surface. Consecutive dry-cut sections of endosperm tissue, ~1.5–2 μm thickness, were cut to include bran layers, aleurone layer, outer vitreous endosperm and inner floury endosperm, and also embryo tissue in T2 and T3. However, cutting of sections sometimes led to loss of the embryo and often part of the floury region of the endosperm. The sections could then be imaged directly using optical and FTIR microscopy.

2.2. Optical microscopy

For optical microscopy, sections were placed on a drop of water on a glass microscope slide, excess water removed and the samples dried (30 °C). Sections were stained with dilute iodine solution (KI/I_2). This was prepared by dissolving 0.2% (w/v) of iodine in a 2% potassium iodide solution. This mixture was then diluted 2:1 with distilled water. Stained sections were viewed and photographed in bright field using an Olympus BX 60 microscope (Olympus, Japan) with ProgRes® Capture Pro 2.1 software (Jenoptik, Germany). Polarised light microscopy images were obtained from unstained and KI/I_2-stained sections.

2.3. FTIR microscopy

For FTIR microscopy, sections were floated on a drop of 70% ethanol on IR-transparent BaF_2 disks (13 mm × 1 mm thick). Excess liquid was removed and the sections dried at ambient temperature and humidity (50–60% RH). IR maps were recorded on a Nicolet iN10 MX FTIR Microscope (Thermo Fisher Scientific, USA) equipped with a 16-element liquid nitrogen cooled mercury cadmium telluride linear array detector. IR maps were measured in transmission with 16 cm^{-1} resolution from 4000 to 715 cm^{-1} in an ultra-fast mapping mode.

The ability to examine thin sections and the absence of autofluorescence allowed for high sample throughput. Initially sections were acquired with 25 μm × 25 μm pixel size, 64 scans and 8 cm^{-1} spectral resolution. Using these parameters it took 6–7 h to image a large section, typically 5 mm × 5 mm for a half kernel section. By experimenting with different acquisition parameters it was established that the same information could be obtained with the ultrafast mapping mode of the spectrometer. This approach uses the same 25 μm × 25 μm pixel size, but requires only one scan at 16 cm^{-1} 'spectral resolution, reducing the time required to obtain maps to only a few minutes.

Overlapping bands were quite broad but this facilitated elimination of noise. However, baseline variations will distort the spectra and impede band height (area) measurements. A range of processing steps was assessed for determining baselines. Automatic baseline correction proved to be unreliable but, because the IR bands are much narrower than broad baseline shifts, the use of derivatives was found to be successful in eliminating a large part of the baseline variations.

Whole sections were scanned at a spatial resolution of 25 μm × 25 μm. Spectra in these maps were baseline corrected and the second derivatives of the baseline-corrected maps were then calculated using the OMNIC Picta™ software. These IR maps were exported to the ENVI V4.8 software package (ITT Visual Information Solutions, Boulder, CO, USA) to map the ratio of the second derivative peaks 1002 and 1041 cm^{-1}, and to calculate average spectra of the inside, outside and edge area within the sections from the baseline-corrected maps (discussed in Section 3.2).

3. Results and discussion

3.1. Optical microscopy of starch granules in KI/I_2 and unstained sections

The individual granules within populations of *wt* maize granules stain blue uniformly with KI/I_2 (Fig. 1b) and show Maltese Cross patterns (Fig. 1c) consistent with a partially-crystalline, radially-aligned internal structure. The amylose concentration is ~30% and the branching distribution of the amylopectin is described by Wang, White, Pollak, and Jane (1993). Different degrees of structural heterogeneity have been reported for *wt* maize starch. Various microscopic studies (see Dhital, Shelat, Shrestha, and Gidley, 2013; and papers cited in this article) illustrate the existence of surface pores and channels into the granules, believed to be of importance in the digestion of the granules with α-amylase. These are macroscopic levels of heterogeneity at the granule level. Microscopic heterogeneity of starch structure within granules has been reported from surface gelatinisation studies of *wt* maize (Jane et al., 2002; Pan & Jane, 2000). These findings were taken to imply an increased concentration of linear amylose chains at the extremities of the granules with increased concentration of branched amylopectin chains with elongated B-chains at the core of the granules. Raman microscopy (Wellner et al., 2011) of *wt* maize kernels yields a map of the ratio of (1-4) and (1-4,6) linked

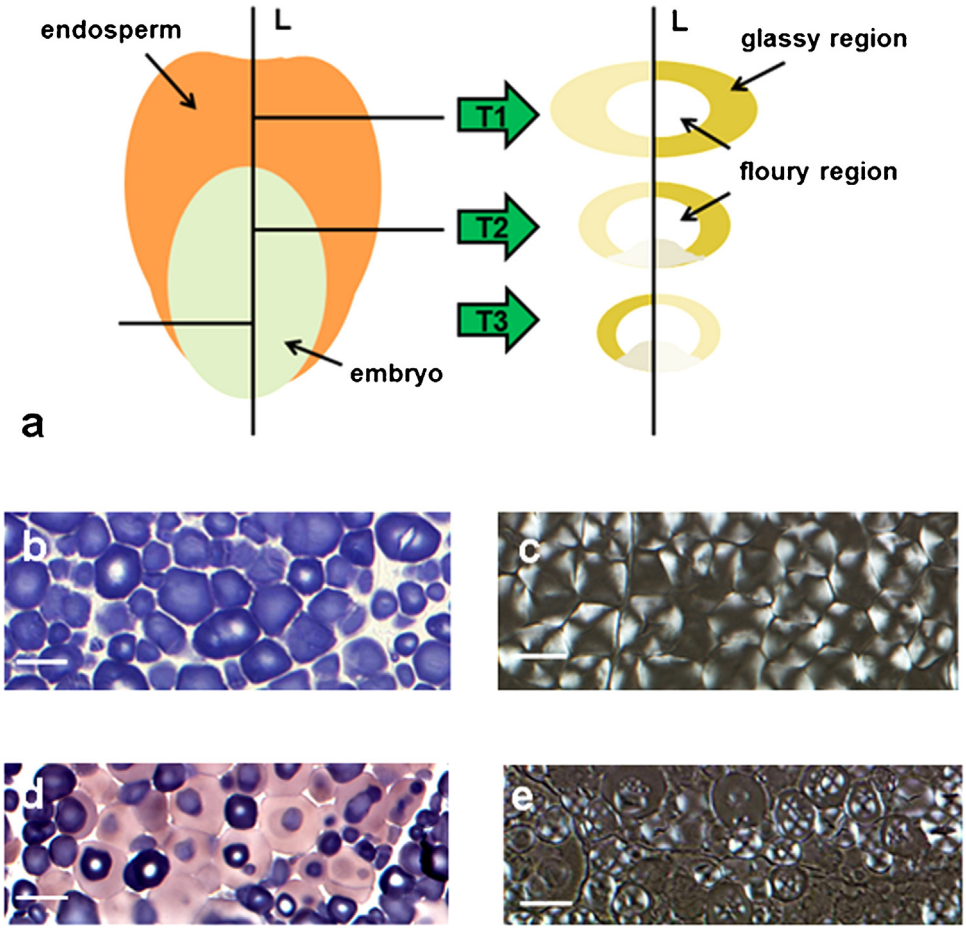

Fig. 1. Sectioning of mature maize kernels. (a) Schematic diagram showing division of the kernel into blocks and location of longitudinal and transverse cuts and sections. (b) KI/I_2-stained section from the inner region of T1 of *wt*. (c) Polarised microscopy image from the inner region of T1 of *wt*. (d) KI/I_2-stained section from the inner region of T1 of *ae*. (e) Polarised microscopy image of the inner region of T1 of *ae*. Bar markers are 10 μm.

glucose within individual starch granules. This ratio was found to be constant across the granule. This result would be consistent with the finding of Jane and co-workers (Jane et al., 2002; Pan & Jane, 2000) if the increased amylose concentration at the outer edge of granule was matched by the increased concentration of B-chains at the core. Moreover, the branching ratio was found to be constant within starch granules across the kernel. Thus the heterogeneity observed by Jane and co-workers (Jane et al., 2002; Pan & Jane, 2000) on populations of isolated starch is characteristic of that for individual granules, although the measured branching distribution for amylopectin will be an average over the entire granule.

The amylose content of the *ae* starch determined by iodine affinity is typically ~46% (Wang et al., 1993). The branching distribution of the amylopectin and the nature of the intermediate material are discussed by Wang et al. (1993). Granules from *ae* mutants are smaller than the spherical granules of *wt* kernels (Liu et al., 2013; Wellner, Parker, Georget, & Morris, 2012), with evidence for a small percentage of elongated or dimpled granules reported previously (Chen et al., 2009; Evans et al., 2003; Jiang, Campbell, Blanco, & Jane, 2010; Jiang, Horner, et al., 2010; Katz et al., 1993; Mercier, Charbonniere, Gallant, & Guilbot, 1970; Wolf, Seckinger, & Dimler, 1964). Elongated structures are reported to be mainly located in the lower inner endosperm regions of the kernel (Boyer, Daniels, & Shannon, 1976a,b). Recent *in situ* studies (Liu et al., 2013; Wellner et al., 2011) on KI/I_2-stained *ae* maize kernels show that granules range in colour from blue throughout (as in *wt*) to biphasic granules containing single or multiple blue-stained regions and a pink outer layer of variable thickness, to granules that appear pink throughout (although the latter are probably biphasic granules sectioned through the pink outer layer). Heterogeneity varies within cells and spatially within the kernel, with the highest heterogeneity in the region where starch deposition begins during kernel development: the inner endosperm region of T1 (Fig. 1d). Various microscopic methods have been used to characterise the molecular structures within the blue- and pink-stained regions and to reveal the underlying ultrastructure (Gérard et al., 2001; Liu et al., 2013; Wellner et al., 2011). The presence of isolated *ae* spherical granules staining uniformly blue with iodine has been reported elsewhere (Evans et al., 2003; Seckinger & Wolf, 1966), and pink-blue heterogeneity has been reported for isolated 'fused' and elongated granules (Cai et al., 2014; Wolf et al., 1964). Because the population of isolated starches is heterogeneous at the molecular level, the measured branching distributions are averages over the population of granule structures and no longer representative of the structures within individual granules.

The *GEMS-0067* starch contains higher levels (~84%) of amylose and the characterisation of the intermediate component and amylopectin is described by Li, Jiang, Campbell, Blanco, and Jane (2008). *GEMS-0067* contains the *ae* gene together with high-amylose modifier (HAM) gene(s). Fig. 2a–f shows representative KI/I_2-stained sections from outer and inner endosperm of *GEMS-0067* from the transverse sampling positions T1–T3 (Fig. 1a). The important observation was that the vast majority of granules in the inner and

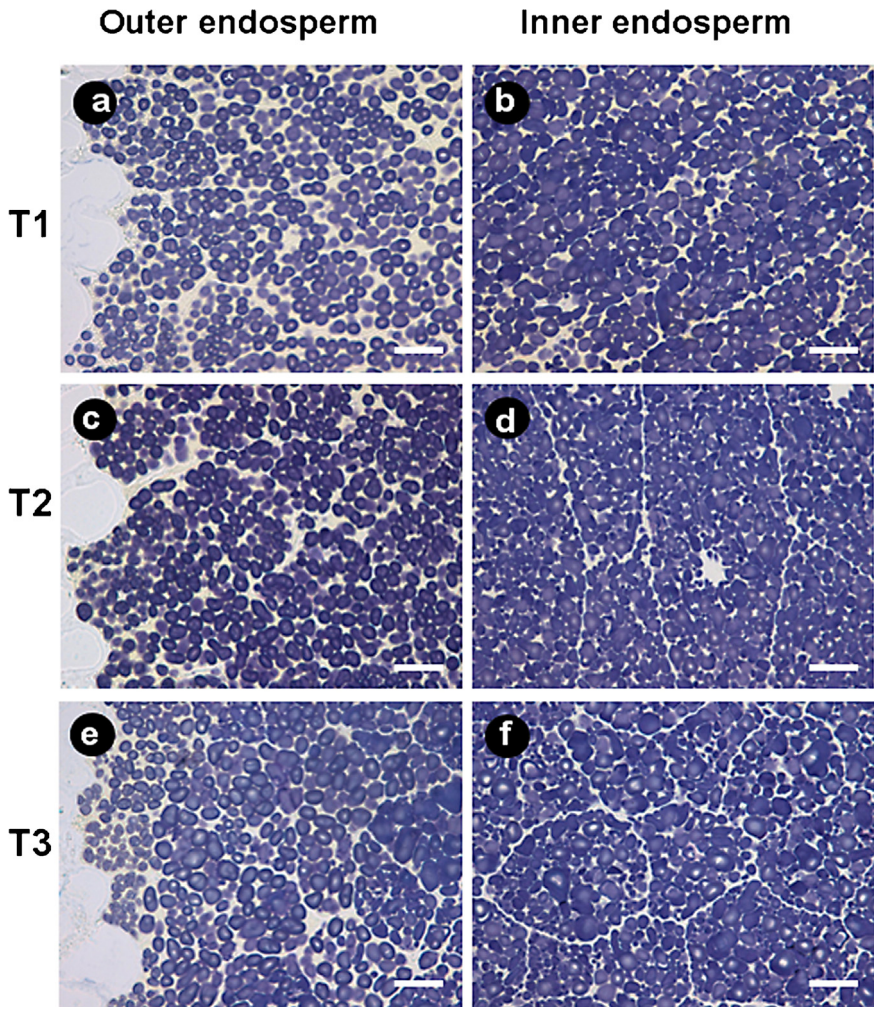

Fig. 2. Representative KI/I2-stained endosperm sections of *GEMS-0067* mutant. (a) T1 outer region. (b) T1 inner region. (c) T2 outer region. (d) T2 inner region. (e) T3 outer region. (f) T3 inner region. Bar markers are 20 μm.

outer endosperm stained blue. Thus the gross structural diversity observed for *ae* was generally absent in *GEMS-0067*. However, if a series of sections are cut near the crown (T1), then some of them reveal the presence of a small amount of biphasic granules (Fig. 3a–c), suggesting a low level of structural heterogeneity characteristic of the *ae* gene, restricted to this part of the kernel. The HAM gene appears to restrict the size of the heterogeneous region observed in *ae* kernels, possibly by causing the boundary transition to largely blue-staining granules to occur earlier during kernel development. For *GEMS-0067* there was a higher degree of heterogeneity in granule size and shape than that for *ae*, which was more pronounced in the inner endosperm region of T3 (Fig. 2f): the degree of shape variation increased from T1 to T3, and thus with growth and development of the kernel. This variation included the presence of elongated rod-like granules, together with the more common spherical granules reported previously (Glaring, Koch, & Blennow, 2006; Jiang, Horner, et al., 2010; Jiang, Lio, Blanco, Campbell, & Jane, 2010), plus rounded larger fused or multiple star-shaped granules. Studies on changes in shape of *GEMS-0067* granules during kernel development (Jiang, Horner, et al., 2010; Jiang, Lio, et al., 2010) reported a general increase in granule size and the presence of more elongated granules at later stages of development after pollination, although these measurements were made on extracted starches.

Fig. 3b and d shows higher magnification views of KI/I_2-stained sections of largely blue-staining *GEMS-0067* granules and illustrates the range of starch morphology in the inner endosperm cells at T1. The section illustrated in Fig. 3b is shown with the addition of crossed-polarisers in Fig. 3d. The blue-staining granules show 'Maltese Cross' patterns (Fig. 3d) indicating radially-aligned ordered structures. The use of the images under crossed polars of stained sections makes it possible to associate any Maltese Cross patterns with specific granules and/or the blue-staining regions within granules. In the present case the Maltese Cross patterns arise from dichroism rather than birefringence. The appearance of Maltese Cross patterns shows that, even if the iodine were to disrupt the crystal structure, it does not disrupt the radial orientation of the starch molecules. Biphasic and fused granules are characteristic of the structures observed in *ae* maize (Liu et al., 2013). Granule structures containing multiple regions of radially-aligned, ordered (crystalline) structures (fused granules) have been reported for high-amylose maize (GEMS-0067) starch (Jiang, Horner, et al., 2010). Transmission electron microscopy studies by Jiang and co-workers (Jiang, Horner, et al., 2010) showed that a small number of amyloplasts contained two starch granules in *wt* maize, and demonstrated that the majority of amyloplasts in *GEMS-0067* mutants contained two or more starch granules. On the basis of these observations it was proposed that the fused elongated structures isolated from *GEMS-0067* containing several radially-aligned, ordered structures, arise from the fusion of individual granules formed in the amyloplast (Jiang, Horner, et al., 2010). A similar explanation was adopted (Liu et al., 2013) to explain the

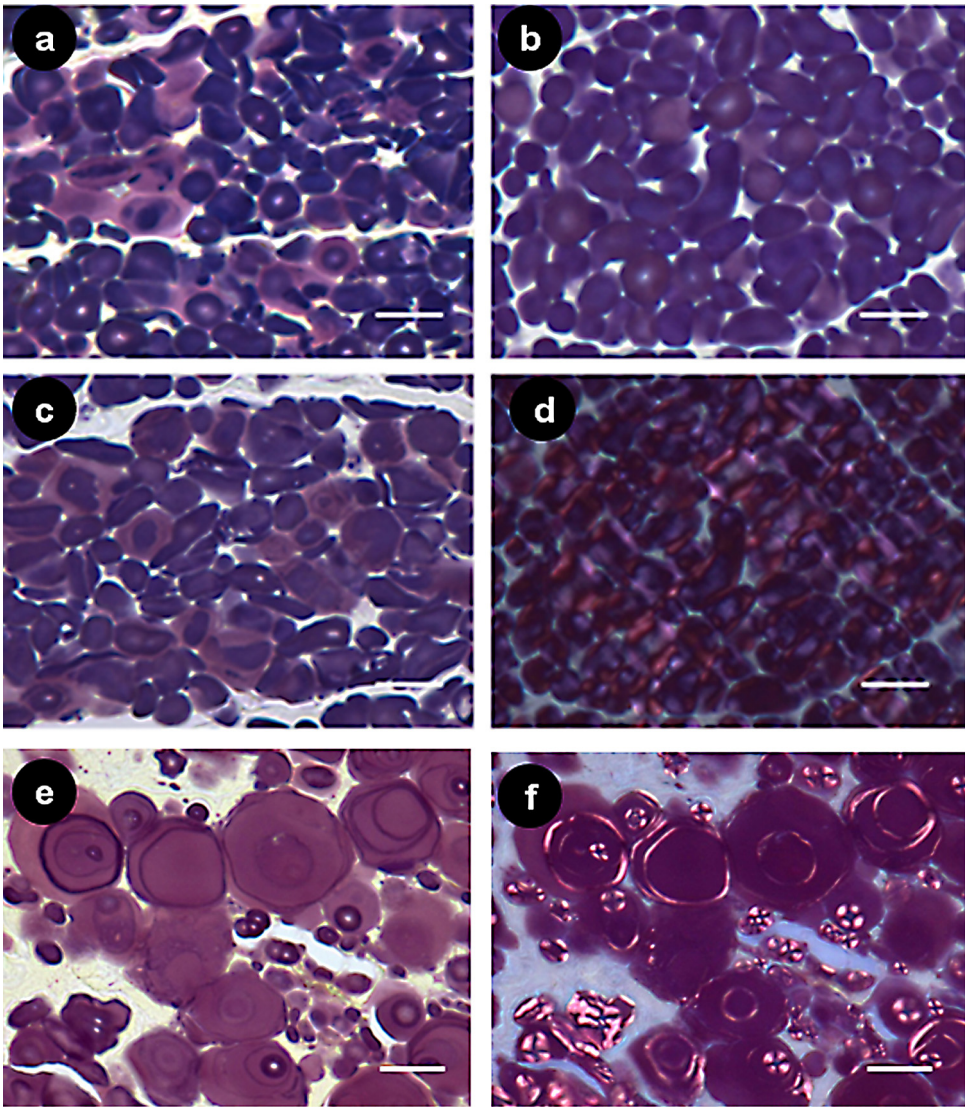

Fig. 3. Higher magnification images of KI/I_2-stained endosperm from the inner region of T1 of double mutants. (a–d) *GEMS-0067* showing characteristic biphasic, spherical and elongated starch granules in bright field, (d) section as in (b) but with the addition of crossed polarisers to show the Maltese Crosses within granules, which are restricted to the blue-staining granules, or the blue regions within fused granules. (e) *wx-ae* section showing biphasic granules. (f) An image of the same section as in (e) but with the addition of crossed polarisers. This image shows that the Maltese Crosses are localised at the central core, in rings within certain granules, or in a thin layer at the surface of certain granules. Bar markers are 10 μm. (For interpretation of the references to color in this figure legend, the reader is referred to the web version of the article.)

complex biphasic structures containing multiple blue-staining regions observed in *ae* single maize mutants. Thus the pink-staining regions present in biphasic granules (Fig. 3a and c) is also the material encasing the blue-staining centres in fused and elongated granules in line with the model proposed for their formation (Jiang, Horner, et al., 2010).

Populations of *wx* granules are homogeneous in the sense that the granules all stain reddish-brown with KI/I_2 and show Maltese Cross patterns consistent with a partially-crystalline, radially-aligned internal structure (Boyer et al., 1976a; Evans et al., 2003; Obanni & BeMiller, 1995). The *wx* granules effectively contain 100% amylopectin (Wang et al., 1993) and a modified amylopectin structure (Jane & Chen, 1992).

The fine structure of amylopectin in *wx-ae* maize starches is described by Yun and Matheson (1993). After KI/I_2 staining, the *wx-ae* mutant structures (Fig. 4) differ from those for *ae* or *wx* starch. Representative images of KI/I_2-stained sections from the outer and inner endosperm at positions T1–T3 are shown in Fig. 4a–f. The granules generally are stained reddish-brown, similar in colour to those of *wx* maize. Closer inspection reveals heterogeneity in the staining of the granules and some degree of heterogeneity in granule size and shape. KI/I_2-staining varies within and between cells within the kernel. In *wx-ae* the majority of the granules in the outer endosperm at position T1 were largely single and spherical or angular in outline. They stained reddish-brown, often with a small blue region around the white (unstained hole) central hilum in the more compact granules (Fig. 4a). Some of the inner endosperm in T1 contained biphasic starch granules, which stained reddish-brown with darker centres (Figs. 3e and 4b). There is evidence for a wider variation in size and shape with some biphasic granules showing multiple centres and concentric rings (Fig. 3e). In addition to the spherical, angular and irregularly-shaped granules, staining reveals that some cells contain groups of much smaller round starch structures, which are evident in Fig. 4d and f. In the inner and outer endosperms of T2 and T3, the colouration of the granules is similar: the granules are stained reddish-brown (as for *wx*) and again the more compact granules stain blue around the hilum (Fig. 4c–f). Granules appear to be mainly spherical with some

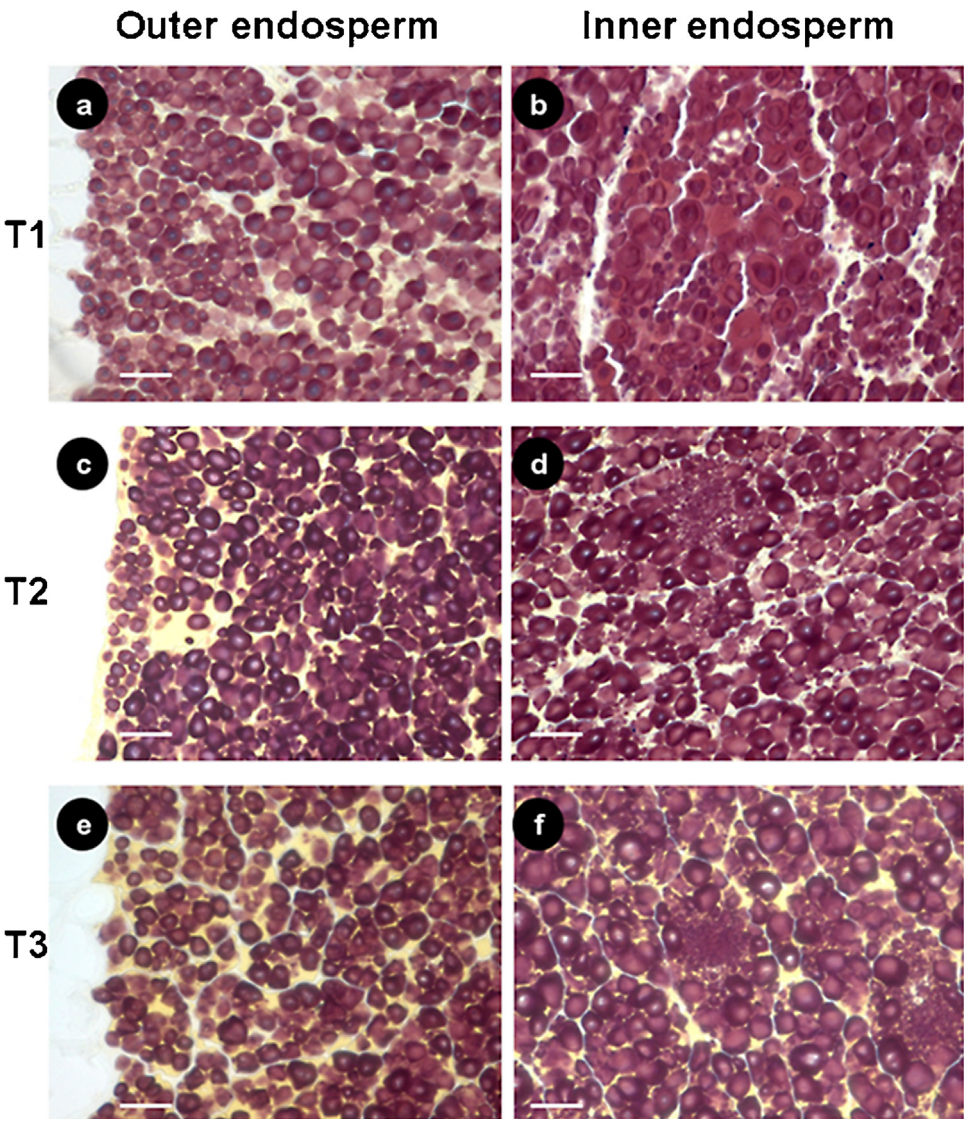

Fig. 4. Representative KI/I_2-stained endosperm sections of *wx-ae* mutant. (a) T1 outer region. (b) T1 inner region. (c) T2 outer region. (d) T2 inner region. (e) T3 outer region. (f) T3 inner region. Bar markers are 20 μm.

angular and elongated structures, and a greater occurrence of small round starch particles.

Polarised light microscopy revealed additional detailed structure of granules within the *wx-ae* kernel. Fig. 3e shows a higher magnification image of the biphasic granules from the KI/I_2-stained inner endosperm at T1. Fig. 3f shows the same section visualised between crossed polarisers. This shows that the variation in staining within granules, although not as marked as the blue-pink transition for pure *ae* mutants, also indicates structural inhomogeneity. Central darker or blue-staining centres show Maltese Crosses, for single or multiple centres, whereas the surrounding regions show no evidence for radially-aligned ordered structure. In some cases radial alignment reappears at the outer edges of granules, and sometimes in darker-stained rings within the granule. The largely spherical granules within T2 and T3 endosperm regions exhibit conventional Maltese Cross patterns (not shown) indicating radially-aligned ordered structures. There were also a few examples of multiple Maltese Cross patterns suggestive of fused granules.

The *wx-ae* mutant shows similar structural heterogeneity to *ae* mutants, with variations within cells and spatially within the kernel, with the highest level of heterogeneity in the region where starch is first deposited during kernel development. The nature of the ordered structure is dominated by the *ae* mutation. The *wx* mutation appears to moderate contrast in the KI/I_2-staining, possibly by affecting the diffusion of the stain as it penetrates into the sections.

The complexity of the *wx*-ae starch structures shows that the population of isolated starches will be heterogeneous. Hence detailed information on the characterisation of starch structure will be an average value for the population and not representative of the structure within individual granules. Further ultrastructural studies and chemical mapping are required to visualise and characterise the variation of starch structure within granules, between cells and within the kernel. The intention was to investigate double mutants in the Oh 43 background but the present data is in a different genetic background and it is possible that other genetic variation in non-starch genes may have indirectly affected starch structures. Thus it would be useful to compare further this double mutant in the Oh 43 background.

3.2. FTIR microscopy

Use of very thin (1.5–2 μm) endosperm sections makes it possible to obtain spectra in transmission mode with a FTIR microscope.

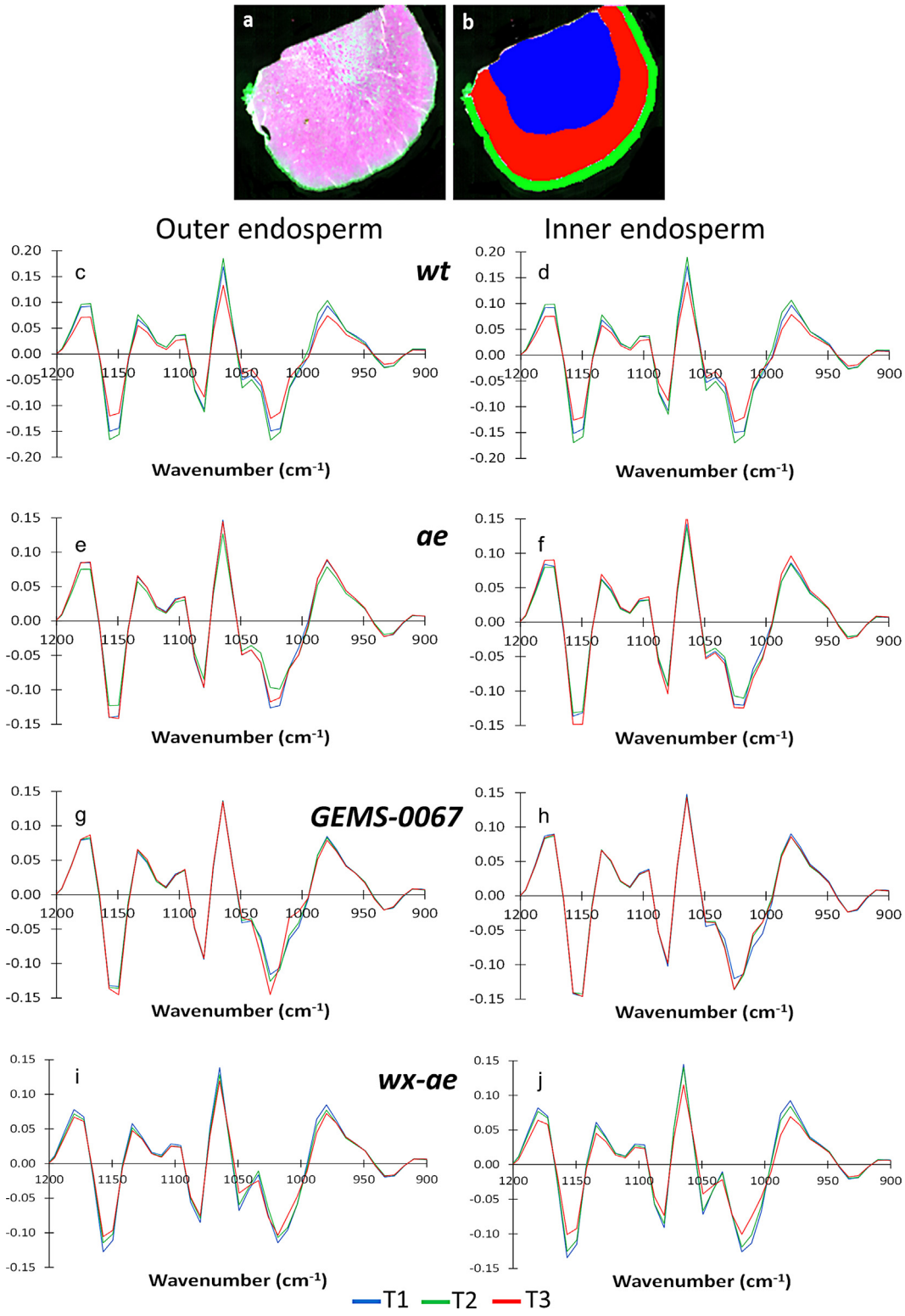

Fig. 5. FTIR maps of endosperm sections. (a) Representative IR map from T1 in the *ae* mutant, (b) the regions for calculating the average IR spectra, inside area blue, outside area red, edge area green. (c–j) Starch bands in the 2nd derivative average FTIR spectra (1200–900 cm^{-1}) from the outer and inner endosperm regions of maize kernel sections from positions T1 to T3. The spectra shown are from *wt* (c and d), and the *ae* (e and f), *GEMS-0067* (g and h), and *wx-ae* (i and j) mutants. (For interpretation of the references to color in this figure legend, the reader is referred to the web version of the article.)

Fig. 5a and b shows schematic diagrams of maps of maize sections and areas from which average spectra were obtained. Although the spatial resolution (*ca* 10 μm, limited by diffraction) was insufficient to resolve individual granules, it was possible to monitor average starch structure within individual cellular regions within the kernel. Previous studies showed that *ae* mutant starch had a very similar infrared spectrum to *wt* (Liu et al., 2013; Wellner et al., 2011). The only real differences were slightly smaller absorption at 1047 cm^{-1}, indicating less ordered (crystalline) structure, and increased adsorption at 1002 cm^{-1} linked to an A- to B-type

starch transition (vanSoest, Tournois, deWit, & Vliegenthart, 1995). In general, single and double mutants containing the *ae* mutation show a tendency to revert from A- to B-type crystals (Gérard, Planchot, Buleon, & Colonna, 1999). Hence mapping the changes in the bands at 1002 and 1047 cm^{-1} should provide evidence for differences between the *wx-ae*, *ae*, *GEMS-0067* mutants and the *wt* maize starches. It is of interest to assess how HAM gene(s) in *GEMS-0067* modifies the structural heterogeneity caused by the *ae* gene.

Differences in spectra for *wt* and *ae* were not immediately obvious in the overall band shape of the strongly-overlapping starch bands in the 1200–900 cm^{-1} region, and only became evident after the use of signal processing techniques such as Fourier deconvolution. By plotting normalised absorbance ratios of these bands as FTIR maps, it was possible to visualise the distribution of starch structures in *wt* and *ae* endosperm sections. These maps showed a large and consistent difference between *wt* and *ae* starches in the nature and degree of ordered starch structure. However, the maps also showed variation within *ae* sections, which may be linked to local variations in granule morphology (Wellner et al., 2012).

In the present study FTIR microscopy has been used to map structural variations in double mutant maize sections.

The strongest bands in the spectra originated from starch. Fourier deconvolution of the 1200–900 cm^{-1} region resolved bands at 1153, 1126, 1105, 1078, 1050, 1044, 1023, 1002, 933 and 924 cm^{-1}. The assignment of these peaks is discussed elsewhere (Wellner et al., 2012). Peaks at 1153, 1105, and 1023 cm^{-1} were the strongest visible negative bands in the 2nd derivative spectra (sharp peaks in the original spectra). The 1078 cm^{-1} band was also resolved as a smaller negative peak. However, the bands at 1050 and 1002 cm^{-1} were only fully resolved at spectral resolutions of 8 cm^{-1} and better. At the 16 cm^{-1} resolution used for these survey maps, the bands at 1050 and 1002 cm^{-1} formed shoulders on either side of the strong 1023 cm^{-1} band.

Fig. 5 shows 2nd derivative FTIR spectra in the starch band region 900–1200 cm^{-1}, averaged from different regions of the kernel depicted schematically in Fig. 5a and b. The spectra for *wt* in the sections T1, T2 and T3 looked practically identical, and also the curves for inner and outer endosperm of these sections were almost superimposable (Fig. 5c and d). This indicated the same starch structure across the whole kernel, which is an excellent confirmation of the observed uniformity of the granules.

The 2nd derivative spectra from equivalent positions in *ae* maize kernel sections Fig. 5e and f were visibly different from *wt*. Previously it was demonstrated (Wellner et al., 2012) that the *ae* spectra showed a larger 1002 cm^{-1} band (linked to an A- to B-type transition) and also some band broadening, resulting in greater overlap with the main 1023 cm^{-1} band and some absorption around 970 cm^{-1}. A similar change was visible in the second derivative spectra with the main negative band at 1023 cm^{-1} appearing less pronounced and broadened at the 1000 cm^{-1} flank. This change in band shape around 1000–1050 cm^{-1} was the main difference between *wt* and *ae*. Closer inspection also revealed slight variations between spectra from different positions of the *ae* kernel. In particular, the relative intensities of the 1022 cm^{-1} peak and 1000 cm^{-1} shoulder varied in accordance with the previous finding that *ae* starch granules and their structures were not uniform within the kernels.

The (local area average) 2nd derivative FTIR spectra from the equivalent positions in *GEMS-0067* kernel sections Fig. 5g and h showed a similar pattern to that of *ae* maize: the main negative band at 1023 cm^{-1} appeared to be less pronounced and somewhat broader at the 1000 cm^{-1} flank than that observed for *wt* sections, and was also found to vary between spectra from different granule positions. The band at 1023 cm^{-1} was consistently different in value from that seen for the *wt*, but found to be particularly strong in the T1 region where in the *GEMS-0067* kernels the granules stained blue with KI/I_2 and contained fewer biphasic blue-pink staining granules. The difference in the value of this band, when compared to its value in the *wt* was smaller in T2, and hardly visible in T3, in regions that showed enhanced heterogeneity in starch shape and size.

Major difference in starch structure was observed for *wx-ae* samples, which also showed heterogeneity in KI/I_2-staining (Fig. 4). Second derivative spectra showed a marked difference in the 1000–1050 cm^{-1} region compared to *wt*, the main effect being that the 1049 cm^{-1} band became clearly visible (especially in T1 and T2) and the main band moved down to 1018 cm^{-1} (Fig. 5i and j). This indicates a higher crystalline/amorphous ratio. The very strong variation in the band shape between positions within the kernel indicates a large local variability of granule structure. This is consistent with KI/I_2-staining and polarised microscopy observations that the *ae* mutation is dominant, leading to structural heterogeneity of granule structure within the kernel.

The main spectral difference occurred in the 1000–1050 cm^{-1} region, hence interest was focused on mapping changes due to the 1041 and 1002 cm^{-1} bands, for comparison with the patterns seen in granule shapes and KI/I_2 staining.

Fig. 6 shows IR maps of the 1002 cm^{-1}/1041 cm^{-1} ratio in the 2nd derivative FTIR spectra for the kernel sections. The large size of whole kernels made it difficult to cut complete sections with an even thickness of 1.5–2 μm. In addition, sections from T2 and T3 included embryo tissue that tended to detach. Therefore these sections for the most part consisted of pieces ï¿½ or ¼ of the total size. Use of the ratio allows structural heterogeneity of granules throughout the kernel to be probed and should eliminate effects of section thickness or different starch content within sections.

Infrared maps of *wt* endosperm (Fig. 6) are uniform indicative of a homogeneous starch structure (the brighter the area, the higher the 1002 cm^{-1}/1041 cm^{-1} ratio): There was no gradient in the ratio from the aleurone inwards into the central endosperm. Typically spectra from T1 and T3 had an average ratio of 0.8, with a slightly lower average of 0.6 in T2 sections.

The ratio was higher in the *ae* endosperm (Fig. 6), consistent with a transition from A- to B-type crystallinity characteristic of the *ae* mutation (Gérard et al., 1999). Unlike *wt* sections the ratio varied within sections and between sections within the kernel. Average values of this ratio were 0.9 in T1, 1.35 in T2 and 1.2 in T3. The ratio varied across the T1 sections with markedly different values in the outer and inner endosperm. The inner endosperm, which contained the most pink-staining biphasic granules, had a lower ratio than outer endosperm, which contains mostly blue-staining granules. Variability of the ratio was less apparent in T2 and T3, consistent with the nature and distribution of the structural heterogeneity observed by KI/I_2-staining, the birefringence of unstained sections and the dichroism of KI/I_2-stained sections. Because the ratio depends on the level of crystallinity, as well as the type of crystal structure, further data is necessary to explain the differences in the ratio for the inner and outer endosperm regions of T3.

In the *GEMS-0067* mutant sections (Fig. 6) the ratio was uniform with average values of 1.2 in T1, and 1.0 in T2. A greater variation of the ratio was observed in the T3 sections with values varying from 0.65 in the outer endosperm to 0.98 in the inner endosperm. The lack of structural variability in the T1 region is consistent with the reduced heterogeneity observed from the KI/I_2 staining and the polarised light microscopy study on *GEMS-0067* kernels. Variability within T3 is perhaps unexpected, but may result from the variability in size and shape of the granules. In particular the proportion of star-shaped and elongated granules is highest in the inner endosperm of T3. Isolated elongated granules show structural heterogeneity revealed by iodine staining and polarised microscopy (Wolf et al., 1964).

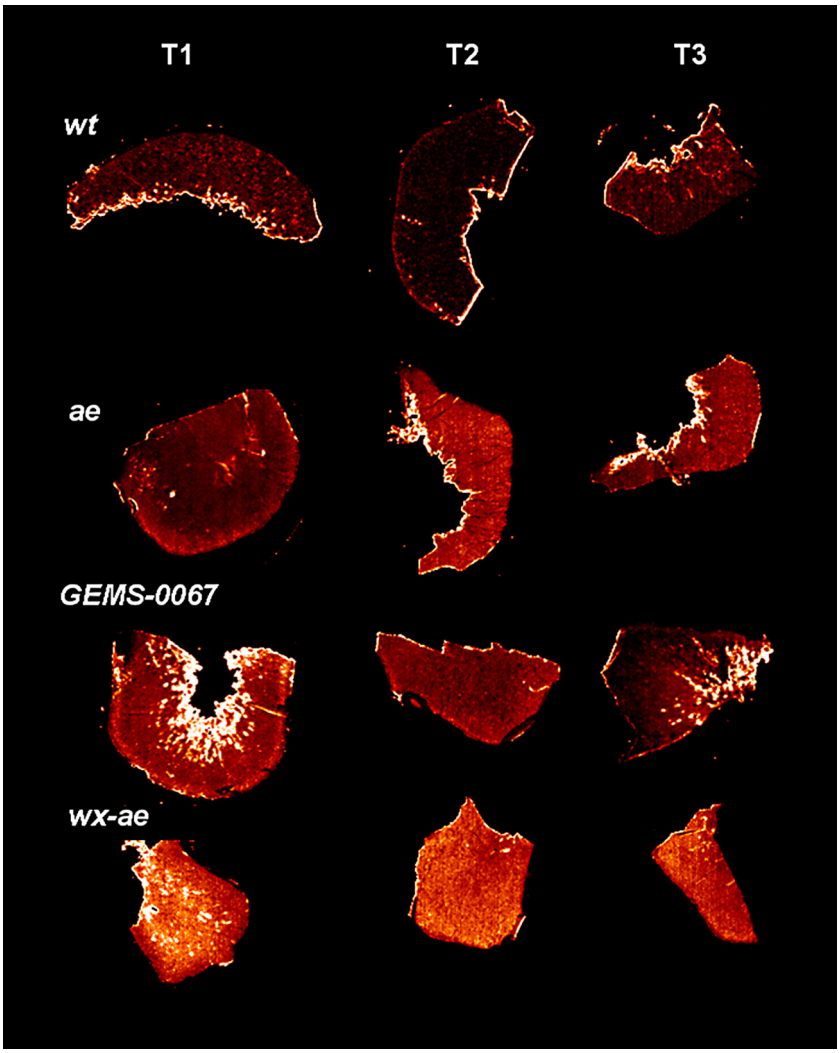

Fig. 6. Infra-red (heat) maps of the 1002 cm^{-1}/1041 cm^{-1} ratio obtained from the second derivative FTIR spectra of endosperm sections from positions T1 to T3 of *wt*, *ae*, *GEMS-0067*, and *wx-ae* kernels.

Maps of *wx-ae* kernels (Fig. 6) revealed the largest changes in starch structure with respect to the maps of *wt* kernels. The ratio varies from 1.8 in the inner endosperm to 1.5 in the outer endosperm of T1 and between 1.6 in the inner endosperm to 1.7 in the outer endosperm of T2 and T3. Changes in the ratio due to the change in crystal form may be smaller than expected, as the loss of amorphous material will decrease the ratio due to the increased crystalline/amorphous value within the granules. The increased value of the ratio is, however, consistent with a transition from A- to B-type crystals and the variation in the ratio within the T1 sections reflects the structural heterogeneity revealed by microscopy. The variability observed in the T2 and T3 sections may once again reflect increased heterogeneity in size and shape observed in these regions of the kernel. In particular there is an increased occurrence of a heterogeneous distribution of small round starch particles within cells in these sections.

Further detailed microscopy studies and chemical mapping are required to reveal the ultrastructural changes responsible for structural heterogeneity in these double mutants.

4. Conclusions

These studies suggest that optical microscopy can be used to reveal structural heterogeneity of starch granule structure *in situ* within *wt* and mutant maize kernels. The method retains the spatial distribution of the starch within the kernel, provides information on the effect of growth and development, and avoids losses, which may occur during starch isolation. Previous studies (Gérard et al., 2001; Liu et al., 2013; Wellner et al., 2011) revealed that changes in staining reflect distinct changes in granule ultrastructure.

The *ae* mutation leads to granule heterogeneity within the kernel (Liu et al., 2013; Wellner et al., 2011). The HAM gene(s) in *GEMS-0067* restrict the size of the heterogeneous region observed for *ae* kernels, but result in an enhanced variation in granule shape and size distributed spatially within the kernel. FTIR and Raman studies reveal increased heterogeneity of *GEMS-0067* likely related to structural heterogeneity of compound granules: such heterogeneity has been reported for elongated starch granules isolated from *ae* mutants.

The *wx* mutation in *wx-ae* mutants results in a pronounced variation in colour induced on staining with KI/I_2. Optical microscopy demonstrates structural heterogeneity of starch granule structure within the kernel equivalent to that observed in the pure *ae* mutant. The *wx* gene leads to an additional variation in granule size and shape, distributed heterogeneously within the kernel.

PCA plots of Raman spectra in the starch region explain the structural differences induced in mutant starches and suggest that

Raman microscopy could be used to map the chemical and physical chemical nature of the starch granule structure.

Acknowledgements

Research between IFR and Zhejiang University was enabled by BBSRC ISIS funding (BB/J004189/1). IFR research was funded through the BBSRC core ISP grant to the Institute. Research at Zhejiang University was supported by the Key Technologies R&D Programme of China (2012BAD29B04) and the Programme for Zhejjang Leading Team of S&T Innovation (2011R50029).

Appendix A. Supplementary data

Supplementary data associated with this article can be found, in the online version, at http://dx.doi.org/10.1016/j.carbpol.2014.11.006.

References

Boyer, C. D., Daniels, R. R., & Shannon, J. C. (1976a). Abnormal starch granule formation in *Zea mays* L. endosperms possessing amylose-extender mutant. *Crop Science*, *16*, 298–301.

Boyer, C. D., Daniels, R. R., & Shannon, J. C. (1976b). Amyloplast development in *Zea mays* L. genotypes affecting kernel polysaccharides. *Plant Physiology*, *57*, 102-102.

Cai, C., Zhao, L., Huang, J., Chen, Y., & Wei, C. (2014). Morphology, structure and gelatinization properties of heterogeneous starch granules from high-amylose maize. *Carbohydrate Polymers*, *102*, 606–614.

Chen, P., Yu, L., Chen, L., & Li, X. (2006). Morphology and microstructure of maize starches with different amylose/amylopectin content. *Starch-Starke*, *58*, 611–615.

Chen, P., Yu, L., Simon, G., Petinakis, E., Dean, K., & Chen, L. (2009). Morphologies and microstructures of cornstarches with different amylose–amylopectin ratios studied by confocal laser scanning microscope. *Journal of Cereal Science*, *50*, 241–247.

Dhital, S., Shelat, K. A., Shrestha, A. K., & Gidley, M. J. (2013). Heterogeneity in maize starch granule internal architecture deduced from diffusion of fluorescent dextran probes. *Carbohydrate Polymers*, *93*, 365–373.

Evans, A., McNish, N., & Thompson, D. B. (2003). Polarization colors of lightly iodine-stained maize starches for amylose-extender and related genotypes in the W64A inbred line. *Starch-Starke*, *55*, 250–257.

Gérard, C., Colonna, P., Bouchet, B., Gallant, D. J., & Planchot, V. (2001). A multi-stages biosynthetic pathway in starch granules revealed by the ultrastructure of maize mutant starches. *Journal of Cereal Science*, *34*, 61–71.

Gérard, C., Planchot, V., Buleon, A., & Colonna, P. (1999). Crystalline structure and gelatinisation behaviour of genetically modified maize starches. In P. Colonna, & S. Guilbert (Eds.), *Biopolymer science: Food and non food applications* (pp. 59–63).

Glaring, M. A., Koch, C. B., & Blennow, A. (2006). Genotype-specific spatial distribution of starch molecules in the starch granule: A combined CLSM and SEM approach. *Biomacromolecules*, *7*, 2310–2320.

Jane, J.-L., & Chen, J.-F. (1992). Effect of amylose molecular size and amylopectin chain length on paste properties of starch. *Cereal Chemistry*, *69*, 60–65.

Jane, J.-L., Ao, Z., Duvick, S. A., Wiklund, M., Yoo, S.-H., Wong, K.-S., et al. (2002). Structures of amylopectin and starch granules: How are they synthesized? *Journal of Applied Glycoscience*, *50*, 167–172.

Jiang, H. X., Campbell, M., Blanco, M. H., & Jane, J. L. (2010). Characterization of maize amylose-extender (ae) mutant starches. Part II: Structures and properties of starch residues remaining after enzymatic hydrolysis at boiling-water temperature. *Carbohydrate Polymers*, *80*, 1–12.

Jiang, H. X., Horner, H. T., Pepper, T. M., Blanco, M., Campbell, M., & Jane, J. L. (2010). Formation of elongated starch granules in high-amylose maize. *Carbohydrate Polymers*, *80*, 533–538.

Jiang, H. X., Lio, J. Y., Blanco, M., Campbell, M., & Jane, J. L. (2010). Resistant-starch formation in high-amylose maize starch during kernel development. *Journal of Agricultural and Food Chemistry*, *58*, 8043–8047.

Katz, F. R., Furcsik, S. L., Tenbarge, F. L., Hauber, R. J., & Friedman, R. B. (1993). Behavior of starches derived from varieties of maize containing different genetic mutations – Effects of starch genotype on granular morphology. *Carbohydrate Polymers*, *21*, 133–136.

Li, L., Jiang, H., Campbell, M., Blanco, M., & Jane, J.-L. (2008). Characterization of maize amylose-extender (ae) mutant starches. Part 1: Relationship between resistant starch contents and molecular structures. *Carbohydrate Polymers*, *74*, 396–404.

Liu, D. L., Parker, M. L., Wellner, N., Kirby, A. R., Cross, K., Morris, V. J., et al. (2013). Structural variability between starch granules in wild type and in *ae* high-amylose mutant maize kernels. *Carbohydrate Polymers*, *97*, 458–468.

Matsushima, R., Maekawa, M., Fujita, N., & Sakamoto, W. (2010). A rapid direct observation method to isolate mutants with defects in starch grain morphology in rice. *Plant and Cell Physiology*, *51*, 728–741.

Mercier, C., Charbonniere, R., Gallant, D., & Guilbot, A. (1970). Development of some characteristics of starches extracted from normal corn and amylomaize grains during their formation. *Starch-Starke*, *22*, 9–16.

Obanni, M., & BeMiller, J. N. (1995). Identification of starch from various maize endosperm mutants via ghost structures. *Cereal Chemistry*, *72*, 436–442.

Pan, D. D., & Jane, J. (2000). Internal structure of normal maize granules revealed by chemical surface gelatinisation. *Biomacromolecules*, *1*, 126–132.

Parker, M. L., Kirby, A. R., & Morris, V. J. (2008). In situ imaging of pea starch in seeds. *Food Biophysics*, *3*, 66–76.

Pérez, S., & Bertoft, E. (2010). The molecular structures of starch components and their contribution to the architecture of starch granules: A comprehensive review. *Starch-Starke*, *62*, 389–420.

Seckinger, H. L., & Wolf, M. J. (1966). Polarization colors of maize starches varying in amylose and genetic background. *Starch-Starke*, *18*, 1–5.

vanSoest, J. J. G., Tournois, H., deWit, D., & Vliegenthart, J. F. G. (1995). Short-range structure in (partially) crystalline potato starch determined with attenuated total reflectance Fourier-transform IR spectroscopy. *Carbohydrate Research*, *279*, 201–214.

Wang, Y.-J., White, P., Pollak, L., & Jane, J. (1993). Characterization of starch structures of 17 maize endosperm mutant genotypes with Oh43 inbred line background. *Cereal Chemistry*, *70*, 171–179.

Wellner, N., Georget, D. M. R., Parker, M. L., & Morris, V. J. (2011). In situ Raman microscopy of starch granule structures in wild type and ae mutant maize kernels. *Starch-Starke*, *63*, 128–138.

Watson, S. A. (1987). Structure and composition. In S. A. Watson, & P. E. Ramstad (Eds.), *Corn: Chemistry and technology* (2nd edition, pp. 53–82). St-Paul, MN, USA: American Association of Cereal Chemists.

Wellner, N., Parker, M. L., Georget, D. M. R., & Morris, V. J. (2012). Raman and FT-IR microscopy of native and high-amylose maize starch *in situ*. In P. A. Williams, & G. O. Phillips (Eds.), *Gums and stabilisers for the food industry 16* (Vol. 335) (pp. 11–18). RSC Special Publications.

Wolf, M. J., Seckinger, H. L., & Dimler, R. J. (1964). Microscopic characteristics of high-amylose corn starches. *Starch-Starke*, *16*, 375–380.

Wu, Y. S., Campbell, M., Yen, Y., Wicks, Z., & Ibrahim, A. M. H. (2009). Genetic analysis of high amylose content in maize (*Zea mays* L.) using a triploid endosperm model. *Euphytica*, *166*, 155–164.

Yun, S. H., & Matheson, N. K. (1993). Structures of the amylopectins of waxy, normal, amylose-extender, and wx-ae genotypes and of the phytoglycogen of maize. *Carbohydrate Research*, *243*, 307–321.

Zhu, L. J., Dogan, H., Gajula, H., Gu, M. H., Liu, Q. Q., & Shi, Y. C. (2012). Study of kernel structure of high-amylose and wild-type rice by X-ray microtomography and SEM. *Journal of Cereal Science*, *55*, 1–5.